AIAA JOURNAL
Vol. 35, No. 3, March 1997

Vortex-Oscillation Model of Airfoil Side-Edge Noise

R. Sen*
Boeing Commercial Airplane Group, Seattle, Washington 98124

Oscillation of the edge vortex is proposed as a mechanism for sound production at the lateral edge of a loaded airfoil. Flow in a spanwise cross section near the edge is idealized by potential flow around a square corner, and the time-averaged edge vorticity is represented by a single line vortex perpendicular to the plane of the flow. Based on a stability requirement, we calculate vortex oscillation modes with frequencies dependent on circulation, edge thickness, and mean distance from the edge. Realistic numbers for these parameters give frequencies that are consistent with measured noise and surface pressure frequencies. Reasonable surface pressure amplitudes are also predicted when experimental estimates of vortex oscillation amplitude are used. Interaction with large flow structures is simulated by perturbing the base vortex with a smaller vortex. This produces pressure spectra with broad peaks, as observed in experiments. The mechanism for broadening is nonlinear dynamics with transition to chaos. Far-field pressure is governed by the speed at which the center of vorticity moves normal to the wall. This previously obtained result is explained by a simple image argument. In a single-vortex model of the edge vorticity, noise production may be reduced by moving the equilibrium position far from the wall; this suppresses the normal component of the vortex-oscillation eigenvector. In multiple-vortex models, noise production may be suppressed by promoting antisymmetric motion. This occurs when the edge-vorticity field is compact or is positioned far from the wall.

I. Introduction

In many modern airplanes, the airframe or nonpropulsive component contributes a significant part of the total noise radiated to the ground during approach. It has been shown that a large and often dominant airframe noise source resides at the lateral edges of part-span trailing-edge flaps. This has been referred to as the flap side-edge noise source.[1,2] This paper presents a simple new conceptual model of the side-edge noise phenomenon.

Theoretical models of this source were first proposed by Hardin[3] and Meecham,[4] who represented the lateral edge of a wing by a two-dimensional knife edge and square corner, respectively. A two-dimensional potential flow sweeping around the edge or corner represented the familiar rollup flow observed in such regions, and a small point vortex convecting with the flow simulated turbulence. The incompressible field of the vortex is converted into far-field sound through scattering by the edge. It was shown that sound production is most intense when the vortex accelerates around the corner; thus, the path followed by an idealized patch of turbulence was shown to be a potentially important determinant of noise. Later, Howe[5] considered a more realistic three-dimensional geometry and concluded that important installation effects can arise from the presence of a main wing close to the active flap edge.

In this paper, we continue along the lines of Hardin's model but add a steady base vortex to the potential flow around a thick edge. This vortex is an idealized representation of the time-averaged vorticity field that resides near lateral edges. Zilliac et al.[6] and Chow et al.[7,8] have measured various flow quantities near the lateral edge of a loaded NACA 0012 airfoil. Their measurements illustrate the spatial development of the edge vortex that is associated with the flow of air from the pressure surface to the suction surface. Considering transverse planes at successive streamwise stations, they show that a sheetlike vorticity distribution in upstream planes develops into a relatively compact distribution within about half the chord of the airfoil. A schematic representation is given in Fig. 1. McInerny and Meecham[9] and others also identify a secondary edge vortex that merges with the main vortical region near the trailing edge.

The present model may be thought of as a first-order representation of the local flow in planes where the vortical region is compact. To our knowledge, the edge vortex has not yet been considered explicitly in models of side-edge noise. Thus, we advance the two-dimensional model as a first step toward understanding its role in sound generation. Although much is undoubtedly lost in a two-dimensional representation, we present concepts that seem applicable in more sophisticated models as well. We also show that certain qualitative and quantitative predictions of the model are generally in agreement with measurements.

Adding a base vortex to the edge flow results in a new conceptual picture of side-edge noise, principally with respect to unsteady near-field mechanisms that may result in sound production. We argue that the base vortex must reside nominally near a position of stable equilibrium in the edge flow. Disturbances to this base system then result in vortex oscillations, and this sets up a fluctuating flowfield near the edge of the airfoil. Thus, the natural dynamics of the base flow, consisting of the rollup flow and base vortex, is seen to play a potentially major role in determining the characteristics of radiated sound.

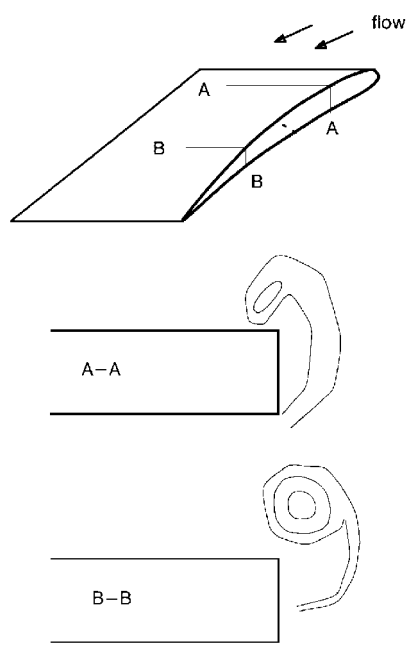

Fig. 1 Schematic representation of a lateral-edge flowfield, showing the rollup of a sheetlike vortical region; lines correspond to contours of constant cross-flow velocity.

Received June 13, 1996; revision received Nov. 27, 1996; accepted for publication Dec. 10, 1996; also published in *AIAA Journal on Disc*, Volume 2, Number 2.

*Specialist Engineer, Noise Engineering, M.S. 67-ML, P.O. Box 3707. Member AIAA.

As in Hardin's[3] and Meecham's[4] work, we also consider a smaller perturbing vortex. The perturbing vortex simulates a large-scale flow structure that may develop, for example, in the lower portions of the edge-vorticity distribution (Fig. 1), perhaps in response to boundary-layer disturbances from upstream locations. We find that the motion of the base vortex is at least as important as that of a perturbing vortex. From the two-vortex system, we are also able to draw some conclusions about the dynamics and acoustics of more general multivortex systems in such edge flows. The latter may be thought of as an extension of the present model in which the (distributed) base vorticity is represented by a number of point vortices. We show that the dynamics of the two-vortex system has chaotic regimes, as may be expected[10]; this gives rise to the broad spectral peaks that are observed in field quantities. We also recognize the existence and causes of a certain canceling pattern in two-vortex oscillations. This has an important influence on far-field noise levels. Both features may be generalized to multivortex systems.

For acoustic calculations, we use informal matching arguments based on the method of matched asymptotic expansions.[11] This assumes a large wavelength/edge thickness ratio, which is consistent with predicted vortex frequencies. Our main goal here is to identify features of the vortex dynamics that provide leading-order contributions to the acoustic field. We find that the usual $\sin(\theta/2)$ directivity for acoustic pressure is recovered for all vortex motions. We also encounter Howe's[12] result that a vortex produces sound mainly when it cuts across base flow streamlines near an edge. A simple physical explanation is found to underlie this phenomenon. For a single-vortex system, we show that this acoustically productive lateral motion depends on the original equilibrium position of the vortex: it is small for equilibrium positions very close to the edge or close to the linear stability boundary (about 0.73 times the edge thickness). And for higher-order multivortex models, we are able to suggest that antisymmetric modes of oscillation result in weak far fields. It is shown that such modes are expected to predominate when the vortex system is compact or positioned far from the wall. Both this and Howe's[12] result represent possible noise-control strategies.

II. Vortex Dynamics

A. General Formulation

We consider a two-dimensional edge of thickness h in the z plane (Fig. 2). Using the Schwartz–Christoffel transformation

$$z(\zeta) = (h/\pi)[\log(\zeta + \sqrt{\zeta^2 - 1}) - \zeta\sqrt{\zeta^2 - 1}] \tag{1}$$

the edge is mapped into the real ζ axis and the region outside the edge into the upper-half ζ plane. Here $-\pi < \arg(\log Z) \leq \pi$ and $0 \leq \arg(\sqrt{Z}) < \pi$ for complex Z. In the ζ plane, a uniform flow with complex potential $-V_0\zeta$ is added to simulate the rollup flow in the z plane. A point vortex of circulation Γ is placed at $\zeta = b$ and its image, $-\Gamma$, at $\zeta = b^*$. This satisfies the impermeability condition on the solid surface. Additional vortices may similarly be added to the flow. If there are N vortices of circulation $\Gamma_j = -k_j$ at points $\zeta = \zeta_j$ with corresponding images, the total complex potential is

$$\Phi(\zeta) = -V_0\zeta + \sum_{j=1}^{N} \frac{ik_j}{2\pi} \log \frac{\zeta - \zeta_j}{\zeta - \zeta_j^*} \tag{2}$$

We shall carry the N-vortex formulation up to a point and then discuss the two-vortex and single-vortex cases in greater detail. The single-vortex case may be viewed as a first-order model of the time-averaged vorticity field near side edges. A spatially distributed vorticity field may be simulated by going to larger N.

The complex velocity in the ζ plane is $\mathrm{d}\Phi/\mathrm{d}\zeta$, and dividing this by $\mathrm{d}z/\mathrm{d}\zeta = -(2h/\pi)(\zeta^2 - 1)^{1/2}$ gives the complex velocity in the z plane

$$u - iv = \frac{-(\pi/h)}{2\sqrt{\zeta^2 - 1}}\left[-V_0 + \sum_{j=1}^{N} \frac{ik_j}{2\pi}\left(\frac{1}{\zeta - \zeta_j} - \frac{1}{\zeta - \zeta_j^*}\right)\right] \tag{3}$$

The motion of each point vortex is described by the desingularized fluid velocity at its instantaneous location.[13] For the jth vortex, the singular part is given by its self-induced free-field contribution $(ik_j/2\pi)[z - z(\zeta_j)]^{-1}$. Subtracting the singularity and working in the ζ plane, we find that the motion of the vortex system is governed by

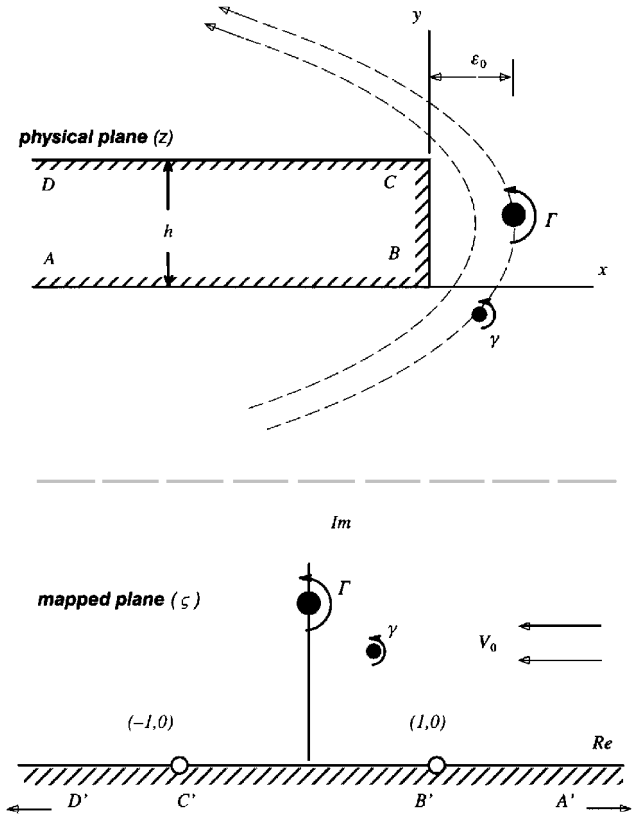

Fig. 2 Edge mapping.

$$\frac{\mathrm{d}\zeta_m^*}{\mathrm{d}t} = \frac{-V_0(\pi/2h)^2}{|\zeta_m^2 - 1|}\left[1 + \frac{s_m}{2\eta_m} + \frac{1}{2}\frac{is_m\zeta_m}{\zeta_m^2 - 1} - \sum_{p\neq m}^{N} is_p\left(\frac{1}{\zeta_m - \zeta_p} - \frac{1}{\zeta_m - \zeta_p^*}\right)\right], \quad m = 1, 2, \ldots, N \tag{4}$$

Here we have used $s_j = k_j/(2\pi V_0)$ and $\zeta_j = \xi_j + i\eta_j$. The system (4) is autonomous, and thus a direct phase-plane interpretation is possible with ξ_j, η_j as phase-plane coordinates. In the z plane, Eq. (4) may be expressed in Hamiltonian form.[13] In the ζ plane, we find that the quantity

$$\mathcal{H} = \sum_{m=1}^{N}\left[s_m\eta_m + \frac{s_m^2}{4}\log|\eta_m^2|\zeta_m^2 - 1|\right] - \frac{1}{2}\sum_{m=1}^{N}\sum_{p\neq m}^{N}\log\left|\frac{\zeta_m - \zeta_p}{\zeta_m - \zeta_p^*}\right| \tag{5}$$

satisfies

$$\frac{\mathrm{d}\xi_m}{\mathrm{d}t} = \frac{r_m}{s_m}\frac{\mathrm{d}\mathcal{H}}{\mathrm{d}\eta_m}, \qquad \frac{\mathrm{d}\eta_m}{\mathrm{d}t} = -\frac{r_m}{s_m}\frac{\mathrm{d}\mathcal{H}}{\mathrm{d}\xi_m}, \qquad r_m = -\frac{V_0(\pi/2h)^2}{|\zeta_m^2 - 1|}$$

Thus, the total derivative $\mathrm{d}\mathcal{H}/\mathrm{d}t$ is zero and, consequently, $\mathcal{H}$ is a constant of the motion. The last obtained equations transform to Hamiltonian form in the z plane. We see that every equilibrium configuration $(\zeta_1, \zeta_2, \ldots, \zeta_N)$ corresponds to a stationary point of $\mathcal{H}$. An equilibrium point will be stable to small perturbations if it is surrounded by closed isosurfaces of $\mathcal{H}$ (that is, if $\mathcal{H}$ attains a strict local extremum at the point. When such closed surfaces exist, they represent the phase-plane manifolds along which oscillatory motion can take place. We note that the only way in which system (4) may respond stably to a small perturbation is to oscillate around its equilibrium point, because Hamiltonian systems do not admit sinks or sources in the phase plane.[14] We use constancy of $\mathcal{H}$ as a check on numerical computations.

B. Single-Vortex System

For a base-flow with one vortex at $\zeta_0 = \xi_0 + i\eta_0$ with strength $\Gamma = -2\pi V_0 s$, the summation term in Eq. (4) drops out, and the equilibrium condition reads

$$1 + \frac{s}{2\eta_0} + \frac{1}{2}\frac{is\zeta_0}{\zeta_0^2 - 1} = 0 \tag{6}$$

There are two families of solutions,

$$\xi_0 = 0, \qquad s = -2\eta_0\frac{1+\eta_0^2}{1+2\eta_0^2} \tag{6a}$$

and

$$s = -\tfrac{4}{3}\eta_0, \qquad \xi_0^2 + \eta_0^2 = 1 \tag{6b}$$

Next, we linearize Eq. (4) and investigate stability to small disturbances. Let δ denote small displacements of the vortex from ζ_0. The linear equation of motion is then

$$\frac{\mathrm{d}\delta^*}{\mathrm{d}t} = \frac{V_0(\pi/2h)^2}{|\zeta_0^2 - 1|}\left[\frac{s\,\mathrm{Im}(\delta)}{2\eta_0^2} + \frac{is\delta}{2}\frac{1+\zeta_0^2}{(\zeta_0^2-1)^2}\right] \tag{7}$$

Setting δ proportional to $\exp(\lambda t)$, we find that λ has either two real roots or two imaginary roots of opposite sign. The first possibility gives us exponential growth and, thus, instability. This is not acceptable because it implies that the base vortex would escape to infinity when subjected to flow perturbations. The second possibility gives oscillatory dynamics, and this is the one we choose. We find that only family [Eq. (6a)] of equilibrium positions satisfies the necessary conditions, provided $\eta_0 < 1$. Denoting the linear oscillation frequency by f and substituting for s from Eq. (6a), we get

$$f = \frac{\Gamma}{32h^2}\frac{\sqrt{(1+\eta_0^2+2\eta_0^4)(1-\eta_0^2)}}{\eta_0(1+\eta_0^2)^3}; \qquad 0 < \eta_0 < 1 \tag{8}$$

This equation is displayed in Fig. 3 along with a curve relating the ζ-plane coordinate η_0 to the corresponding nondimensional distance ε_0/h in the physical plane. Note that vortex equilibrium positions occur on the line of symmetry $\xi_0 = 0$ or $y = h/2$. The farthest stable position, $\eta_0 = 1$, corresponds to $\varepsilon_0/h \approx 0.73$.

To derive numbers from Eq. (8), we first consider parameters typical for a $\frac{1}{15}$-scale model of a medium-sized commercial transport airplane. We take $\Gamma = 2$ m^2/s; this is estimated from the jump in the sectional lift distribution curve at the flap edge. For thickness, we take $h = 0.01$ m. This represents the thickness of the flap at its leading edge. The frequency f is then Γ/h^2 or 20 kHz times the value of the nondimensional parameter fh^2/Γ, which depends on η_0. We discuss two ways in which a value of η_0 may be chosen.

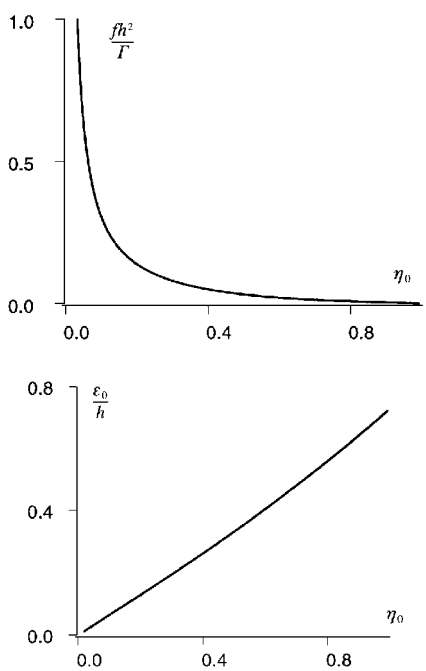

Fig. 3 Single-vortex oscillation frequency and equilibrium position.

Because velocities go to infinity at the corners $\zeta = \pm 1$, one way to choose η_0 is to require that the unperturbed base flow satisfy the Kutta condition at $\zeta = \pm 1$. Note from Eq. (6a) that η_0 is fixed once s, the nondimensional circulation, is specified. However, $s = -\Gamma/(2\pi V_0)$, and the parameter V_0 does not seem to relate to any physical quantities that we may estimate by simple means. The Kutta condition offers a way out of this difficulty by fixing the value of s. The Γ in our model may be viewed as the circulation of the outboard streamwise vortex filament in a lifting-line model of the flap, and as such it should be considered given. Thus with s and Γ as external inputs to the model, we have a way to choose the nonphysical V_0. Note that in contrast to two-dimensional airfoil theory, the Kutta condition does not determine circulation in this scheme. From Eq. (3), the condition of zero v gives

$$-1 - 2s\,\mathrm{Im}[1/(\zeta - \zeta_0)] = 0$$

for points ζ on the boundary. Setting $\zeta = \pm 1$ and choosing an equilibrium location $\zeta_0 = i\eta_0$ for the vortex, we find that

$$s = -\frac{1+\eta_0^2}{2\eta_0}$$

Comparing this with the expression in Eq. (6a) for equilibrium positions, we see that the two formulas agree when $\eta_0^2 = \frac{1}{2}$ or $\varepsilon_0/h \approx 0.485$. This location lies within the linear stability boundary. For the parameters chosen, the corresponding oscillation frequency is about 260 Hz. We show later that the far-field acoustic signature is characterized by the vortex oscillation frequency and its harmonics. Thus, we may turn directly to noise data to compare frequencies. We consider data recorded with a directional microphone, which allows us to distinguish the flap-edge noise source from other parts of an airframe. For the model transport airplane, we find that the flap-edge source is active between a few hundred hertz to about 10 kHz, with pronounced spectral peaks at the lower end starting at about 800 Hz. The oscillation frequency predicted for the Kutta position is, thus, of the correct order of magnitude. In that sense, the proposed mechanism appears viable, despite the drastic idealizations introduced in the theoretical model.

Obviously, these idealizations limit the accuracy of the model, and thus it is inappropriate to take the Kutta equilibrium position and corresponding oscillation frequency too literally. Data from Refs. 6–8 are a reminder of these limitations: if we estimate a center for the edge-vorticity field in their data, we find that it does not lie on the line of symmetry, as predicted here. It is worth estimating the range of frequencies associated with these experimental equilibrium positions. Thus, we choose ε_0/h based on an eye estimate of the center of vorticity and calculate the corresponding η_0. In effect, this is an alternative method for fixing V_0. From the Ref. 6–8 data, we find that ε_0/h is about $O(1)$. Consider a range of about 0.2–0.7 for ε_0/h: the lower limit is probably set by vortex core size, whereas the upper limit is set by linear stability. The corresponding range for η_0 is about 0.3–0.96 and for fh^2/Γ is about 0.08–0.0025. For the transport airplane model, this corresponds to frequencies between 50 Hz and 1.6 kHz, which lie at the lower end of the measured spectra, as mentioned earlier.

In the Chow et al.[7] experiments, much lower frequencies, on the order of a few hertz, are estimated. These also appear to be consistent with our model. Chow et al.[7] gives chord $c = 1.22$ m, freestream $U_\infty = 51.8$ m/s, and $\Gamma/(U_\infty c) = 0.33$ for a 10-deg angle of attack. Taking $h = c/10$ to be a representative thickness, we find $f \approx 18$ Hz for the Kutta position. This low value can be explained by the relatively small value of Γ/h^2, about 0.9 kHz. The airplane model data, on the other hand, correspond to a thin, highly loaded flap system. Thus, it stands to reason that Γ/h^2 is much larger in that case. As a final comparison of Eq. (8) with data, we consider surface pressure spectra measured by McInerny and Meecham[9] (it is shown subsequently that surface pressure spectra may also be dominated by the vortex oscillation frequency). These data also correspond to a

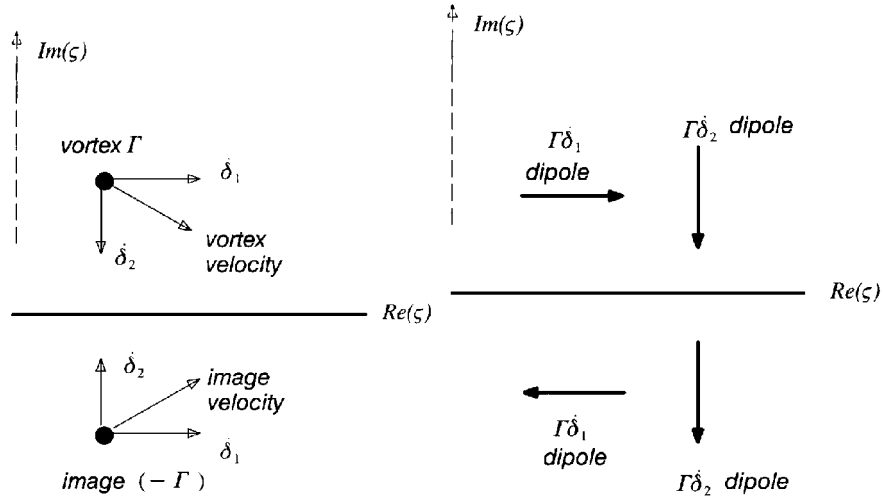

Fig. 4 Incompressible dipole vectors (right panel) associated with motion of vortex and its image (left panel) in mapped plane (ζ); horizontal dipoles oppose each other, whereas vertical dipoles reinforce.

NACA 0012 section, as in the Chow et al.[7] experiment. Scaling the Chow et al. value of $\Gamma/(U_\infty c)$ linearly with angle of attack α, we find thickness-based Strouhal numbers fh/U_∞ of 0.52 and 0.69 for $\alpha = 12$ and 16 deg, respectively (for the Kutta-position oscillation frequency). These estimates give the correct order of magnitude: surface pressure spectra in McInerny and Meecham's[9] Figs. 5 and 6 are seen to peak at Strouhal numbers of about 0.5–2.0.

Next we consider how vortex oscillation frequencies show up in field quantities. We consider pressure, which is typically measured in the far field and also on the flap surface.[1,9] The pressure is given by

$$-p = \varrho_0 \frac{v^2}{2} + \varrho_0 \frac{\partial \phi}{\partial t}$$

up to a constant, where ϱ_0 is density, v the fluid velocity magnitude, and $\phi = \mathrm{Re}(\Phi)$ the potential. Let us first consider points on the surface of the flap edge. Using Eq. (3) with $N = 1$ and noting that ζ is real on the surface, we write

$$v \approx \frac{(\pi V_0/h)}{2\sqrt{\zeta^2 - 1}}\left[1 + 2s\,\mathrm{Im}\left(\frac{1}{\zeta - \zeta_0 - \delta(t)}\right)\right]$$

For equilibrium positions not too close to the edge, we may write for $|\delta| \ll |\zeta - \zeta_0|$

$$v \approx \frac{(\pi V_0/h)}{2\sqrt{\zeta^2 - 1}}\left[1 + 2s\,\mathrm{Im}\left(\frac{1}{\zeta - \zeta_0} + \frac{\delta}{(\zeta - \zeta_0)^2}\right)\right]$$

Squaring this expression, we see that the leading-order time-dependent term will be proportional to $\delta(t)$. Thus, for small perturbations, the dynamic head $\varrho_0 v^2/2$ will fluctuate with essentially the same time dependence as the vortex oscillation. The rate of change of potential is found from Eq. (2). We get

$$\frac{\partial \Phi}{\partial t} = -iV_0 s\left[\frac{\dot{\delta}(t)}{\zeta - \zeta_0 - \delta(t)} - \frac{\dot{\delta}^*(t)}{\zeta - \zeta_0^* - \delta^*(t)}\right] \tag{9}$$

and thus to leading order,

$$\frac{\partial \phi}{\partial t} = \mathrm{Re}\frac{\partial \Phi}{\partial t} \approx 2V_0 s\,\mathrm{Im}\left(\frac{\dot{\delta}(t)}{\zeta - \zeta_0}\right) \tag{10}$$

This component of dynamic pressure is proportional to the speed $\dot{\delta}(t)$ of the vortex and, therefore, it is 90 deg out of phase with the fluctuating dynamic head. Note that large streamwise correlation lengths are typically found in wall pressure spectra.[4,9] This feature seems consistent with a vortex-oscillation model, the present two-dimensional model being a simple version thereof.

Similar conclusions apply for points distant from the edge. For distant points we can generalize to both large and small vortex motions because $|\delta| \ll |\zeta|$ for all reasonable δ and thus the preceding approximations apply. Note, however, that the dynamic head drops off like $|\zeta|^{-6}$ or $|z|^{-3}$ with distance, whereas the fluctuating potential decays at the much smaller rate of $|\zeta|^{-1}$ or $|z|^{-1/2}$. Thus, the fluctuating potential will dominate in the far field and ultimately drive the acoustic pressure, as discussed in Sec. III.

We see, moreover, that for large $|\zeta|$

$$\frac{\partial \Phi}{\partial t} = -iV_0 s\left[\frac{\dot{\delta}}{\zeta - \zeta_0 - \delta} - \frac{\dot{\delta}^*}{\zeta - \zeta_0^* - \delta^*}\right] \approx \frac{2V_0 s\,\mathrm{Im}(\dot{\delta})}{\zeta} \tag{11}$$

so that only that part of the fluctuating pressure that is associated with $\mathrm{Im}(\dot{\delta})$, or motion across the edge-flow streamlines, leaks out to the far field. This result was derived by Howe.[12] We show here that this phenomenon may be understood as an interaction between the vortex and its image. Writing the first term inside the large brackets as

$$\frac{\partial \Phi}{\partial t} = -\frac{iV_0 s\dot{\delta}}{\zeta - \zeta_0 - \delta} \approx \frac{\Gamma}{2\pi}\frac{\dot{\delta}_1 + i\dot{\delta}_2}{\zeta - \zeta_0}$$

we see that the motion $\dot{\delta}_1 = \mathrm{Re}(\dot{\delta})$ simulates a fluctuating incompressible dipole oriented along $\xi = \mathrm{Re}(\zeta)$, that is, parallel to the boundary, and $\dot{\delta}_2 = \mathrm{Im}(\dot{\delta})$ a dipole normal to the boundary. The image vortex must have the same $\dot{\delta}_1$ but is associated with a Γ of opposite sign. Thus, the two ξ-oriented dipoles will tend to cancel, forming an incompressible quadrupole. However, the product $\Gamma\dot{\delta}_2$ is the same for both the vortex and its image, and thus the η-oriented normal dipoles reinforce each other. This is shown in Fig. 4.

Anticipating the coupling between the incompressible far field and the acoustic field, we may thus consider ways in which the magnitude of $\dot{\delta}_2(t)$ may be suppressed. In the small-disturbance analysis, this magnitude will depend on the magnitude of the initial disturbance and on the inclination between the disturbance vector and the eigenvector or modal vector of the vortex system. We may, generally, consider these parameters difficult to control and thus concentrate on finding regimes in which the eigenvector itself has a low relative level of $\dot{\delta}_2(t)$. Because $\dot{\delta}_1(t)$ and $\dot{\delta}_2(t)$ share the same time factor, we may compare $\delta_1(t)$ and $\delta_2(t)$ instead. From Eq. (7), we find that

$$\left|\frac{\delta_1}{\delta_2}\right| = \sqrt{\frac{1 + \eta_0^2 + 2\eta_0^4}{\eta_0^2(1 - \eta_0^2)}}$$

Thus, flat orbits with motion predominantly parallel to the boundary occur for equilibrium positions close to the wall and for positions close to the stability boundary $\eta_0 = 1$. This is illustrated by the numerical computations in Fig. 5. We show two orbits in the ζ plane, one corresponding to an equilibrium position of $\eta_0 = 0.01$ and the other to $\eta_0 = 0.5$. Both cases were started with an initial perturbation of $\delta_1 = 0.01$ and $\delta_2 = 0$.

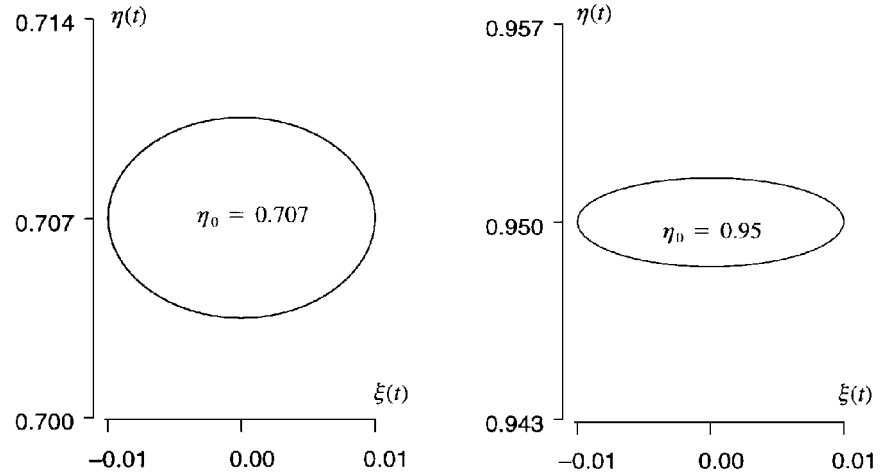

Fig. 5 Orbits in the mapped plane.

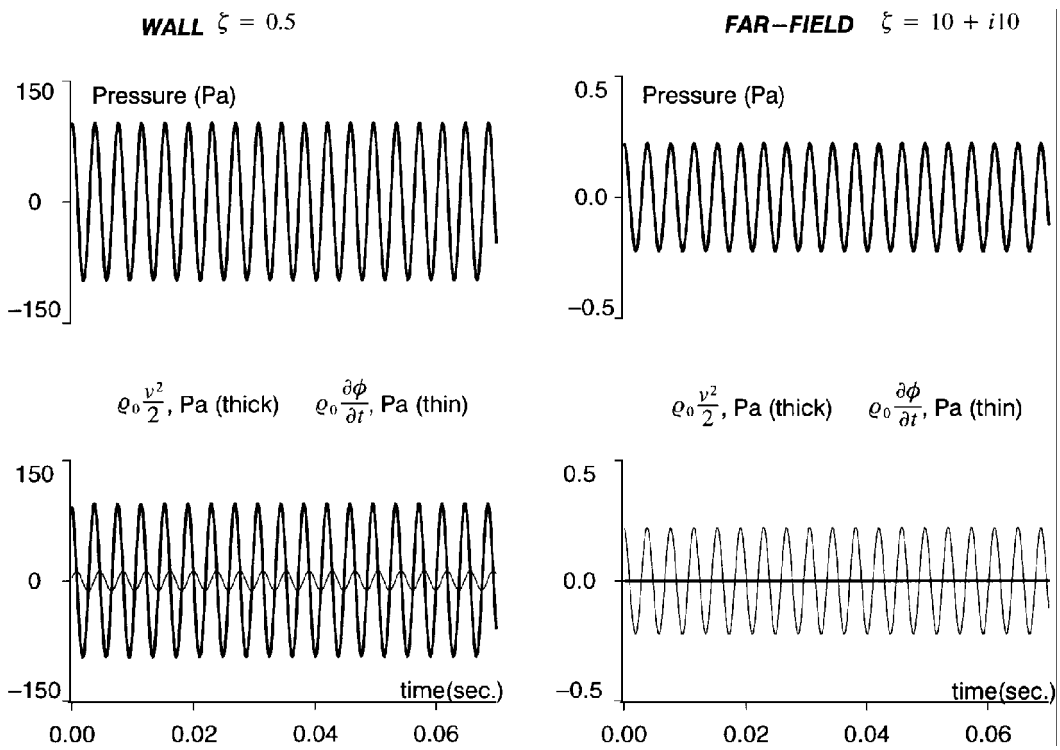

Fig. 6 Fluctuating pressure and its components at a wall location and at a far-field location.

We also show plots of pressure and related quantities for the $\eta_0 = 0.5$ case in Fig. 6. Two measurement locations are taken: one on the wall at $\zeta = 0.5$ and the other in the far field at $\zeta = 10 + i10$. For p and $\varrho_0 \partial\phi/\partial t$ in these plots, we have subtracted time-averaged values. The features discussed earlier are clearly visible in the figure. Note that wall pressure fluctuations are on the order of 100 Pa or about 130 dB referred to 20 μPa. The corresponding oscillation amplitudes are of the order of $|d\zeta| \approx 0.003$, or $|dz| \approx 0.002h$ in the physical plane. Chow et al.[7] estimate vortex meander amplitudes of the order of 10^{-4} times the chord of their NACA 0012 airfoil. Taking a representative thickness $\frac{1}{10}$ the chord, we get $|dz| \approx 0.001h$ in their experiment. We have seen that for small motions, pressure fluctuation magnitudes scale with oscillation amplitudes. Thus, for $|dz| \approx 0.001h$, wall pressure fluctuations of about 50 Pa may be estimated. Turning to McInerny and Meecham's NACA 0012 data,[9] we see that this is the correct order of magnitude. From their Table 1, we find that rms pressure normalized by $\varrho_0 U_\infty^2/2$ lies between 0.02 and 0.08 for various points on the surface. Using their middle speed of $U_\infty = 55$ m/s and taking $\varrho_0 = 1.2$ kg/m^3, we get a range of about 36–145 Pa. High fluctuating pressures may result from very small vortex motions.

C. Small Perturbing Vortex

Next we consider the effect of introducing a much smaller point vortex as a perturbing agent. Let us think of the two-dimensional model as representative of flow conditions in a short streamwise segment. Then the perturbing vortex may be thought of as a large-scale structure that enters the flow domain from an upstream location. There are generally two kinds of interaction in the two-dimensional model. One possibility is that the perturbing vortex escapes to infinity after disturbing the base system. We may interpret this as an escape to a larger orbit in an adjacent flow domain. In this case, the base vortex soon settles down to its natural dynamics, which we have already covered. It may be interesting, however, to study what happens when such perturbing vortices are introduced randomly. A second possibility is that the perturbing vortex enters into a joint oscillatory system with the base vortex. This is the case we study through some numerical examples. In a strictly two-dimensional picture, vortex trapping cannot go on indefinitely, for that effectively adds to the base vorticity, which would then grow without bound. In a three-dimensional setting, however, a trapped vortex would also leave the flow domain in a finite amount of time.

Table 1 Initial conditions for the orbits of Fig. 7

Orbit	$\xi_1(0)$	$\eta_1(0)$	$\xi_2(0)$	$\eta_2(0)$
1	0.100000000000000*E*−02	0.302000000000000*E*+00	0.980000000000000*E*+00	0.100000000000000*E*−01
2	0.125000000000000*E*−02	0.301000000000000*E*+00	0.955000000000000*E*+00	0.136717403168972*E*−01
3	0.150000000000000*E*−02	0.300000000000000*E*+00	0.930000000000000*E*+00	0.156585074619124*E*−01
4	0.175000000000000*E*−02	0.299000000000000*E*+00	0.905000000000000*E*+00	0.167465837195377*E*−01

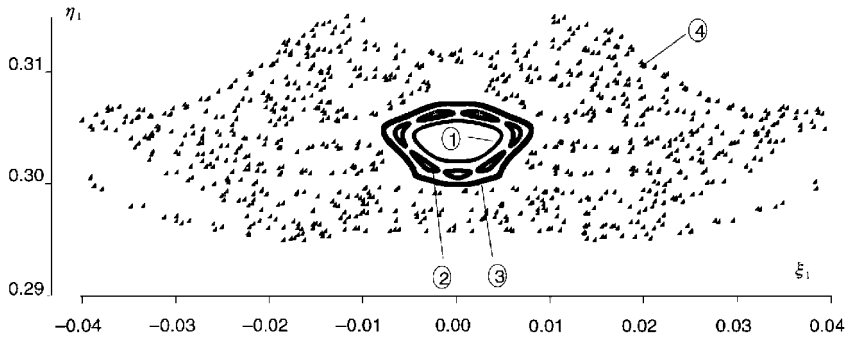

Fig. 7 Poincaré sections for the two-vortex system; four different initial conditions corresponding to the same value of $\mathcal{H}$; 1, 2, 3: regular trajectories, 4: chaotic trajectory; equations integrated up to $t = 0.2$ s.

Another reason for studying the two-vortex system is that we are able to make some generalizations to the dynamics of general multi-vortex systems. A natural extension of the present model is to represent the edge-vorticity field as a system of many point vortices. We find features in the noise production by the two-vortex system that are pertinent to noise production by multi-vortex systems as well.

In the following examples, we take $\Gamma = 2\ \mathrm{m}^2/\mathrm{s}$ for the base vortex and $\gamma = \Gamma/100$ for the perturbing vortex. We choose $\eta_0 = 0.3$ for Γ and determine s from Eq. (6a); this also determines V_0. The base vortex is initially at some $\xi_1(0) + i\eta_1(0)$, close to its nominal equilibrium position, and the perturbing vortex is at some $\xi_2(0) + i\eta_2(0)$, close to the wall. We study a set of initial conditions corresponding to a fixed value of $\mathcal{H}$. The Hamiltonian can be identified with the finite part of kinetic energy.[13] Thus, in a sense, these initial conditions represent equal-energy initial configurations of the vortex system. Coordinates $\zeta_1(t)$ and $\zeta_2(t)$ describe the time-dependent positions of the large and small vortices, respectively.

Generally, perturbing vortices escape when they are introduced close to the wall in $|\xi_2(0)| \gtrsim 1$, although there are initial positions in $|\xi_2(0)| \lesssim 1$ as well for which the small vortex may escape after a few orbits around the base vortex. When the small vortex is trapped, its influence can change dramatically with different initial conditions. This is illustrated by the Poincaré sections in Fig. 7. The figure shows the instantaneous position of Γ at times when $\dot{\xi}_2(t) = 0$ and $\ddot{\xi}_2(t) > 0$; that is, it is a conditionally sampled history of the position of Γ. Table 1 shows the initial conditions for the orbits of Fig. 7. We see that for the first three cases in the figure, points fall on smooth curves, indicating regular motion. In the fourth case, the points fill up a two-dimensional region, indicating chaos.[15] Note that all four cases correspond to the same energy and also that very small changes in initial conditions cause large qualitative changes in the dynamics. From the sequence of closed curves (cases 1 and 3) and island chains (case 2) in Fig. 7, it appears that the route to chaos is consistent with the standard Hamiltonian scenario.[15]

Corresponding orbits for the base vortex are shown in Fig. 8. The nominal single-vortex frequency for Γ is about 1600 Hz. Because γ is small, one of the fundamental frequencies of the linearized two-vortex system might be expected to be roughly 1600 Hz. In Fig. 9, we show far-field spectra for three cases. It appears that this fundamental frequency and its harmonics are present in all cases. There appears to be a second fundamental frequency as well, possibly related to the second mode of the linearized system. All three cases are nonlinear, because the small vortex undergoes large motions. Thus, the dominant peaks are not very sharp in either case; this remains true even for smaller frequency-analysis bins. In the chaotic case, there is further broadening in the high-frequency part of the spectrum. Thus, we may say that the present model includes a

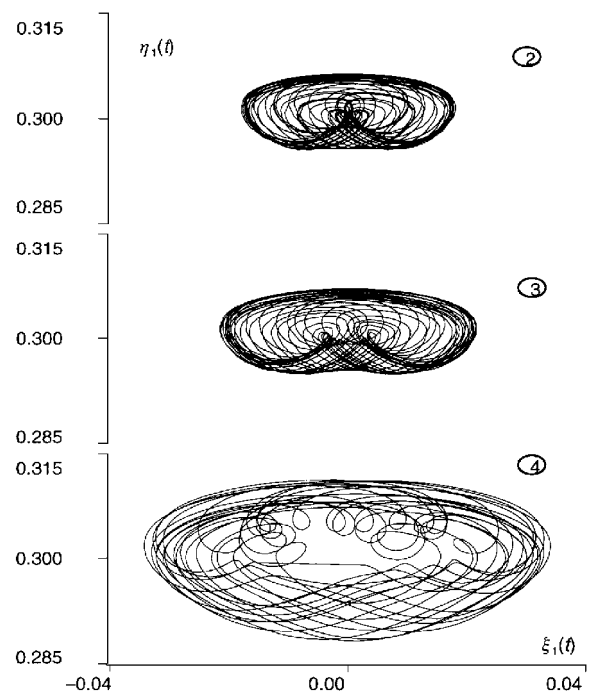

Fig. 8 Perturbed orbits of the base vortex; trajectory numbers correspond to Fig. 7.

mechanism for spectral broadening. Wall pressure spectra measured by McInerny and Meecham[9] show a broad dominant peak, followed by smaller, also broad peaks. This feature is partly seen in case 4 of Fig. 9.

A further point of interest is the relative contribution of each vortex to the far-field pressure. In Fig. 10, we compare the time rate of change of potential due to each vortex, because these are the components that survive in the far field. The rate of change of complex potential due to Γ is %

$$\frac{\partial \Phi^{(1)}}{\partial t} = \frac{i\Gamma}{2\pi}\left[\frac{\dot{\zeta}_1}{\zeta - \zeta_1(t)} - \frac{\dot{\zeta}_1^*}{\zeta - \zeta_1^*(t)}\right]$$

and that due to γ is

$$\frac{\partial \Phi^{(2)}}{\partial t} = \frac{i\gamma}{2\pi}\left[\frac{\dot{\zeta}_2}{\zeta - \zeta_2(t)} - \frac{\dot{\zeta}_2^*}{\zeta - \zeta_2^*(t)}\right]$$

We show the real parts of these quantities multiplied by ϱ_0. It is found that in every case, including the chaotic one shown in the figure, there is a tendency for the two contributions to cancel. This is remarkable considering the great disparity in vortex strengths and also the very nonlinear regimes this feature persists through. It turns out that the phenomenon follows from a simple property of vortex motion.

Letting $|\zeta| \to \infty$ in the preceding expressions and adding, we get

$$\frac{\partial \Phi}{\partial t} \approx \frac{i}{2\pi\zeta}[(\Gamma\dot{\zeta} + \gamma\dot{\zeta}) - ()^*] \tag{12}$$

The quantity within the first parentheses is proportional to the rate at which the center of vorticity moves. It is well known that for vortices moving under their own influence in free space this quantity is zero.[13] That is, in free space, vortex motions possess a kind of antisymmetry. In the present example, the fact that $\mathrm{Im}(\Gamma\dot{\zeta})$ and $\mathrm{Im}(\gamma\dot{\zeta})$ are approximately antisymmetric points to a tendency toward free-space motion. Conversely, it is the presence of the edge that destroys perfect antisymmetry and, thus, allows pressure fluctuations to leak out into the far field (at this order of approximation). This is an alternate conceptualization of the well-known ability of edges to scatter near fields[2,11] into sound. A possible noise-control strategy is to find ways to promote antisymmetric motion as far as possible. A second way in which $\partial\Phi/\partial t$ in Eq. (12) may be made small is to promote parallel-to-the-wall motion as discussed earlier; that is, suppress the speeds $\dot{\eta}_{1,2}$.

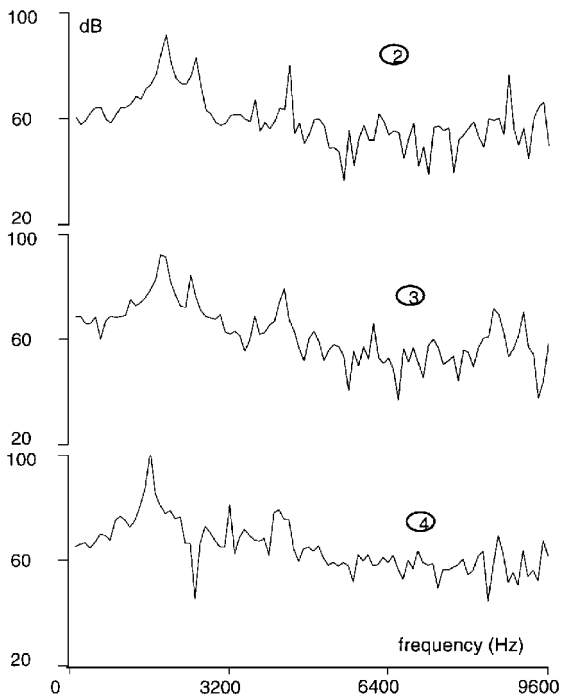

Fig. 9 Amplitude spectrum of incompressible pressure at $\varsigma = 10 + i10$; dB referred to 20 μPa. Bin width is 125 Hz; trajectory numbers correspond to Fig. 7.

From Eq. (4), we see that each vortex moves partly under the influence of its own image, the flow V_0, and the influence of the other vortex and its image. There is also the extra term outside the summation in Eq. (4). Of these, the first two contributions cancel out in Eq. (12) because they do not contribute to motion normal to the wall. Thus, we are left with the interaction term that is represented by the summation in Eq. (4) and the extra term just mentioned. The interaction term is very similar to a free-space interaction term. It is small when we have a compact vortex system with small-amplitude motions.

Let us generalize Eq. (12) to an N-vortex system. The following then applies to an N-vortex model of the edge vorticity. We have

$$\frac{\partial \Phi}{\partial t} \approx -\frac{iV_0}{\zeta}\left[\sum_m^N s_m \frac{\mathrm{d}\zeta_m}{\mathrm{d}t} - \sum_m^N s_m \frac{\mathrm{d}\zeta_m^*}{\mathrm{d}t}\right] \tag{13}$$

Using Eq. (4) and working with normalized circulations s_m, we find

$$\sum_m^N s_m \frac{\mathrm{d}\zeta_m}{\mathrm{d}t} = \sum_m^N r_m \left[s_m + \frac{s_m^2}{2\eta_m} - \frac{1}{2}\frac{is_m^2\zeta_m^*}{\zeta_m^2 - 1}\right]$$

$$+ i\sum_m^n r_m \sum_{p\neq m}\left(\frac{s_m s_p}{\zeta_m^* - \zeta_p^*} - \frac{s_m s_p}{\zeta_m^* - \zeta_p}\right) \tag{14}$$

Here, $r_m = r_m(\zeta_m) = -V_0(\pi/2h)^2|\zeta_m^2 - 1|^{-1}$.

The first term in the double summation resembles a free-space interaction term, except for the ζ_m-dependent factor r_m. If we have a compact distribution of vortices, this factor is approximately constant, and we may move it outside the m summation. In that case, the term with $(\zeta_m^* - \zeta_p^*)$ in the denominator sums to zero on account of antisymmetry. The corresponding term in the second summation in Eq. (13) will likewise have $(\zeta_m - \zeta_p)$ in the denominator and also approximately sum to zero.

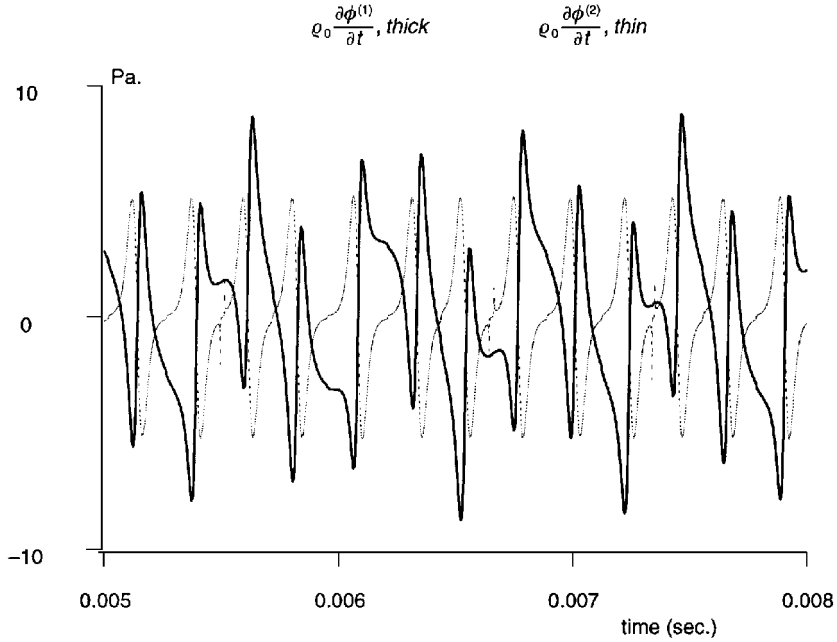

Fig. 10 Components of far-field pressure.

The second term in the double summation of Eq. (14) pairs with its counterpart in Eq. (13) as follows:

$$-i\sum_{m=1}^{n} r_m \sum_{p\neq m}\left(\frac{s_m s_p}{\zeta_m^* - \zeta_p} + \frac{s_m s_p}{\zeta_m - \zeta_p^*}\right)$$

The expression in parentheses is antisymmetric, and again the double summation is approximately zero if the vortex distribution is compact. Finally, the $(r_m s_m)$ and $r_m s_m^2/(2\eta_m)$ terms in Eq. (14) are real and, therefore, they are cancelled by their counterparts from the second summation of Eq. (13). Thus for compact vorticity distributions, the dominant contribution is

$$\frac{\partial\Phi}{\partial t} \approx -\frac{V_0}{\zeta}\sum_{m=1}^{N} r_m(\zeta_m) s_m^2 \,\mathrm{Re}\left(\frac{\zeta_m}{\zeta_m^2 - 1}\right) \tag{15}$$

The real part of this expression is proportional to pressure. We see that it may be made smaller by increasing the distances ζ_m.

To summarize, the incompressible far field due to an N-component edge-vortex system may be suppressed by promoting antisymmetric or centroid-conserving motion. This occurs if the N-vortex system is compact and if individual vortices undergo small motions. In that case, the vortices remain close to each other, move largely under each other's influence, and feel the effects of the wall only weakly. Thus centroid-conserving free-space motion is approximated. Moving the vortex system farther from the wall is also helpful; note this decreases r_m in the given expressions. Finally, motion predominantly parallel to the wall also results in lower pressure levels. If the vortex distribution is very close to the wall, such motion is likely to prevail because of the proximity of the image system. This is essentially the mechanism for the behavior of the single-vortex eigenvector, as discussed earlier. However, positions very close to the wall are probably unlikely because of finite core size.

III. Acoustics

We have implicitly been working within the framework of a low-frequency acoustic formulation. This aspect is now discussed in greater detail. Suppose we restrict attention to radiation frequencies such that the acoustic wavelength is much greater than the flap-edge thickness: $\lambda \gg h$. For the airplane model considered in Sec. II.B, $h = 1$ cm. Let us take $\lambda/h \gtrsim 5$ as a lower limit of validity for low-frequency theory. This corresponds to frequencies of about 7 kHz and lower. For most conditions, this covers at least half of the spectral region considered important for flap-edge noise.

If $\lambda \gg h$, the vortical region near the flap edge occupies a small fraction of the wavelength. For low flow speeds, this justifies an incompressible local flow model to leading order. Far away from the edge where $|z| = O(\lambda)$, we consider fluctuations to be small enough to be modeled by the acoustic equations for still air. Note that in this two-dimensional model, there is no counterpart of a mean flow in the flight direction. We do have a steady flow component due to the V_0 term in Eq. (3). Because this field decays like $|\zeta|^{-1}$ or $|z|^{-1/2}$ for large $|z|$, it is comparable to acoustic magnitudes in the far field. However, it does not affect the acoustic equations because it is steady and incompressible. Let $\boldsymbol{v}_a(t)$ stand for acoustic velocity fluctuations and let $\boldsymbol{v}_i$ represent the steady incompressible field. In the far field, the linear inviscid mass conservation and momentum equations are then

$$\frac{\partial\varrho}{\partial t} + \varrho_0(\nabla\cdot\boldsymbol{v}_a) + \varrho_0(\nabla\cdot\boldsymbol{v}_i) = 0 \qquad \varrho_0\frac{\partial\boldsymbol{v}_a}{\partial t} + \nabla p = 0$$

Since v_i is incompressible, the acoustic approximation is recovered. Furthermore, v_i satisfies the boundary condition on the wall. Thus, we may simply add v_i to the acoustic field when matching acoustic velocities to local flow velocities.

Matching is accomplished by comparing acoustic quantities in the limit $(r/\lambda) \to 0$ to incompressible quantities in the limit $(r/h) \to \infty$, where $r = |z|$. For large $|z|$, the mapping function tends to

$$\zeta \to \sqrt{\pi\frac{r}{h}}\exp\left[\frac{i(\theta+\pi)}{2}\right], \qquad -\pi < \theta = \arg(z) < \pi$$

Using Eq. (13) for an N-vortex system, the incompressible pressure is found to behave like

$$\varrho_0\,\mathrm{Re}\left(\frac{\partial\Phi}{\partial t}\right) \to -\varrho_0\,\mathrm{Re}\left(\frac{1}{\pi\zeta}\sum_{m=1}^{N}\Gamma_m\frac{\mathrm{d}\eta_m}{\mathrm{d}t}\right)$$

or

$$p_i(t) \to \varrho_0\frac{\sin(\theta/2)}{\pi^{\frac{3}{2}}(r/h)^{\frac{1}{2}}}\sum_{m=1}^{N}\Gamma_m\frac{\mathrm{d}\eta_m}{\mathrm{d}t} \tag{16a}$$

as $(r/h) \to \infty$. Here p_i is the incompressible pressure field. Formally taking Fourier transforms, we get

$$\tilde{p}_i(f) \to -2\pi i f\varrho_0\frac{\sin(\theta/2)}{\pi^{\frac{3}{2}}(r/h)^{\frac{1}{2}}}\sum_{m=1}^{N}\Gamma_m\tilde{\eta}_m(f) \tag{16b}$$

where

$$p_i(t) = \int_{-\infty}^{\infty}\tilde{p}_i(f)e^{-2\pi i f t}\,\mathrm{d}f$$

and, similarly, for $\eta_m(t)$, $\tilde{p}_i(-f) = \tilde{p}_i^*(f)$, etc., because all time-domain quantities are real.

In the acoustic field, $r = O(\lambda) \gg h$ and to a first approximation, the flap edge may be considered a knife edge of zero thickness. Thus, we may express the acoustic pressure amplitude $\tilde{p}_a(f)$ in terms of a complete set of outgoing wave functions for the space $-\pi < \theta < \pi$. A set that also satisfies the boundary conditions $\partial/\partial\theta = 0$ on $\theta = \pm\pi$ is[11]

$$H_{n/2}(kr)\begin{Bmatrix}\cos(n\theta/2) & n\ \text{even}\\ \sin(n\theta/2) & n\ \text{odd}\end{Bmatrix}$$

where H refers to a Hankel function of the first kind and $k = 2\pi/\lambda$ is the wave number. From Eq. (16b), we see that only the $n = 1$ wave function is capable of matching the θ dependence of the incompressible far field. Thus, we take

$$\tilde{p}_a(f) \approx a_1(f)H_{\frac{1}{2}}(kr)\sin(\theta/2) \tag{17}$$

The constant $a_1(f)$ is determined by matching the $(r/h) \to 0$ limit of Eq. (17) to the expression in Eq. (16b). Using the small-argument formula

$$H_{\frac{1}{2}}(kr) \to -(i/\pi^{\frac{1}{2}})(kr/2)^{-\frac{1}{2}}$$

we get

$$a_1(f) = 2\pi\varrho_0 f\sqrt{\frac{h}{\pi\lambda}}\sum_{m=1}^{N}\Gamma_m\tilde{\eta}_m(f) \tag{18}$$

Equations (17) and (18) demonstrate the coupling between vortex oscillation amplitudes and the two-dimensional acoustic far field. The incompressible far field depends on vortex motions $\tilde{\eta}_m$ through exactly the same summation term that appears in Eq. (18). Thus, we may apply all our earlier conclusions regarding the incompressible far field to the acoustic field as well.

IV. Summary

We have presented a new conceptual model of airfoil side-edge noise in which oscillation of the edge-vorticity field plays a central role. Various predicted features of near and far fields appear to be consistent with experimental data. Some of these features are oscillation frequency, wall pressure amplitude, large chordwise correlation lengths, and the presence of broad peaks in wall and far-field spectra. It is seen that both natural and forced dynamics of the edge vortex are important. The former sets the fundamental oscillation frequency, whereas the latter provides a mechanism for spectral broadening via nonlinearity and chaos. We also identify features of edge-vortex dynamics that may be useful for noise suppression. One of these features applies to multivortex models of the edge vorticity: we show that when the vortical region is compact or far away from the wall, constituent vortices tend to move in a mutually canceling manner, resulting in low acoustic production. A further strategy is to minimize vortex motion normal to the wall. In a single-vortex model of the edge vorticity, this occurs when the vortex equilibrium location is close to its stability boundary.

Acknowledgments

This work was performed at The Boeing Company under NASA Research Contract NAS1-20090 Task 2. Many thanks are extended to Jeffrey Crouch for reviewing the manuscript and for offering many helpful suggestions and to Yue-Ping Guo for pointing out an error in an earlier version of the manuscript.

References

[1]Miller, W. R., "Flap Noise Characteristics Measured by Pressure Cross-Correlation Techniques," Ph.D. Thesis, Dept. of Mechanical, Aerospace, and Nuclear Engineering, Univ. of California, Los Angeles, CA, 1980.

[2]Crighton, D. G., "Airframe Noise," *Aeroacoustics of Flight Vehicles: Theory and Practice*, edited by H. H. Hubbard, Vol. 1, NASA RP 1258, 1991.

[3]Hardin, J. C., "Noise Radiation from the Side Edges of Flaps," *AIAA Journal*, Vol. 18, No. 5, 1980, pp. 549–552.

[4]Meecham, W. C., "Aerosound from Corner Flow and Flap Flow," *AIAA Journal*, Vol. 21, No. 2, 1983, pp. 228–234.

[5]Howe, M. S., "On the Generation of Side-Edge Flap Noise," *Journal of Sound and Vibration*, Vol. 80, No. 4, 1982, pp. 555–573.

[6]Zilliac, G. G., Chow, J. S., Dacles-Mariani, J., and Bradshaw, P., "Turbulent Structure of a Wingtip Vortex in the Near Field," AIAA Paper 93-3011, July 1933.

[7]Chow, J. S., Zilliac, G. G., and Bradshaw, P., "Measurements in the Near-Field of a Turbulent Wingtip Vortex," AIAA Paper 93-0551, Jan. 1993.

[8]Chow, J. S., Zilliac, G. G., and Bradshaw, P., "Turbulence Measurements in the Near-Field of a Wingtip Vortex," ASME Forum on Turbulence in Complex Flows, Chicago, IL, Nov. 1994.

[9]McInerny, S. A., and Meecham, W. C., "An Experimental Investigation of Wing Tip Turbulence with Applications to Aerosound," AIAA Paper 86-1918, July 1986.

[10]Aref, H., "Integrable, Chaotic, and Turbulent Vortex Motion in Two-Dimensional Flows," *Annual Review of Fluid Mechanics*, Vol. 15, 1983, pp. 345–388.

[11]Crighton, D. G., "Radiation from Vortex Filament Motion Near a Half Plane," *Journal of Fluid Mechanics*, Vol. 51, Pt. 2, 1972, pp. 357–362.

[12]Howe, M. S., "Contributions to the Theory of Aerodynamic Sound, with Application to Excess Jet Noise and the Theory of the Flute," *Journal of Fluid Mechanics*, Vol. 71, Pt. 4, 1975, pp. 625–673.

[13]Saffman, P. G., *Vortex Dynamics*, Cambridge Univ. Press, New York, 1992, Chap. 7.

[14]Bender, C. M., and Orszag, S. A., *Advanced Mathematical Methods for Scientists and Engineers*, McGraw–Hill, New York, 1978, Chap. 4.

[15]Hénon, M., "Numerical Exploration of Hamiltonian Systems," *Chaotic Behavior of Deterministic Systems*, edited by G. looss, R. H. G. Helleman, and R. Stora, USMG/NATO ASI Session 36 (Les Houches, France), North-Holland, Amsterdam, 1983.

S. Glegg
Associate Editor